



Article

Carbon Nanotubes Blended Nematic Liquid Crystal for Display and Electro-Optical Applications

Bhupendra Pratap Singh¹, Samiksha Sikarwar², Kamal Kumar Pandey³, Rajiv Manohar¹, Michael Depriester⁴ and Dharmendra Pratap Singh^{5,*} 

- ¹ Liquid Crystal Research Lab, Department of Physics, University of Lucknow, Lucknow 226007, India; bhupendraphy@gmail.com (B.P.S.); rajiv.manohar@gmail.com (R.M.)
- ² Integrated Basic Science, School of Physical and Decision Sciences, Babasaheb Bhimrao Ambedkar University, Lucknow 226025, India; samiksha9.2009@gmail.com
- ³ Department of Physics, Shri Jai Narain Misra Post Graduate College, Lucknow 226001, India; kamalpande27@gmail.com
- ⁴ Université du Littoral Côte d'Opale, UR 4476, UDSMM, Unité de Dynamique et Structure des Matériaux Moléculaires, 145, Av. Maurice Schumann, 59140 Dunkerque, France; Michael.Depriester@univ-littoral.fr
- ⁵ Université du Littoral Côte d'Opale, UR 4476, UDSMM, Unité de Dynamique et Structure des Matériaux Moléculaires, F-62228 Calais, France
- * Correspondence: dharmendra.singh@univ-littoral.fr; Tel.: +33-(0)3-21-46-57-58

Abstract: In this paper, we investigate a commercial nematic liquid crystal (LC) mixture namely E7 dispersed with small concentrations of multi-walled carbon nanotubes (MWCNTs). The dielectric and electro-optical characterizations have been carried out in the homogeneously and vertically aligned LC cells. The electro-optical response of LC molecules has been enhanced by 60% after the addition of MWCNTs, which is attributed to the reduced rotational viscosity in the composites. MWCNTs act like barricades for ionic impurities by reducing them up to ~34.3% within the dispersion limit of 0.05 wt%. The nematic–isotropic phase transition temperature (T_{NI}) of the E7 LC has also been shifted towards the higher temperature, resulting in a more ordered nematic phase. The enhanced birefringence and orientational order parameter in the LC-MWCNTs are attributed to π - π electron stacking between the LC molecules and the MWCNTs. The outlined merits of the LC-MWCNTs composites evince their suitability for ultrafast nematic-based electro-optical devices.

Keywords: carbon nanotubes; liquid crystal; threshold voltage; electro-optical properties



Citation: Singh, B.P.; Sikarwar, S.; Pandey, K.K.; Manohar, R.; Depriester, M.; Singh, D.P. Carbon Nanotubes Blended Nematic Liquid Crystal for Display and Electro-Optical Applications. *Electron. Mater.* **2021**, *2*, 466–481. <https://doi.org/10.3390/electronicmat2040032>

Academic Editor: Roberto Centore

Received: 15 August 2021

Accepted: 28 September 2021

Published: 8 October 2021

Publisher's Note: MDPI stays neutral with regard to jurisdictional claims in published maps and institutional affiliations.



Copyright: © 2021 by the authors. Licensee MDPI, Basel, Switzerland. This article is an open access article distributed under the terms and conditions of the Creative Commons Attribution (CC BY) license (<https://creativecommons.org/licenses/by/4.0/>).

1. Introduction

Liquid crystal (LC) materials are ubiquitous in everyday life. It has a wide range of commercial applications such as reliable displays for the several electronic devices [1], tunable filters and lenses for ophthalmic applications [2,3], smart windows [4], various components of medical equipment [5], sensors for chemical, biological and satellite applications [6–8], and many more. Generally, thermotropic LCs, in which phase transition is achieved as a function of temperature, are used for aforementioned applications. The nematic phase is the most prevailing phase of thermotropic LCs, which appears just below the isotropic phase upon cooling. At the isotropic–nematic phase transition, the molecular symmetry is reduced from spherical to cylindrical showing an appearance of the long-range orientational order. The concept of Guest–Host mode has been proposed to enhance the physical properties of the pristine LCs [9]. With this consideration, the coupling of nanotechnology with that of the soft condensed mesogens (i.e., LC–nanomaterial composites) have drawn a significant interest from researchers for obtaining superior display and nano-display applications [10].

Based on their ordered structure, carbon nanotubes (CNTs) offer many fascinating properties like polarization, high dielectric constant, etc., that could be utilized in various mechanical and electronic devices [11–14]. During the last two decades, the physical

interactions between the LCs and CNTs has obtained an immense research interest worldwide [15–20]. The addition of small amount of CNTs into the LCs could lead to some fascinating phenomena. Prasad et al. [21] demonstrated that the doping of a small amount of CNT in host nematic LC induces a layered smectic A phase and has also shown the nematic–smectic–nematic re-entrant phase sequence. A combined theory of Flory–Huggins and Landau–de Gennes has been predicted to support these results. In another study, Dolgov et al. [22] have investigated an electro-optical (E-O) memory effect for multiwalled carbon nanotubes (MWCNTs)-doped negative dielectric anisotropic nematic LC system. They noticed that the efficiency of E-O memory depends on morphological networking of CNTs and the efficiency of electro-hydrodynamic flow in LC. Petrov et al. have studied the external magnetic field-induced orientational transitions in nematic-CNT suspension and described the segregation effect of CNTs on the orientation and magneto-optical response of CNTs doped nematic LC [19,23]. The suppression of screening field in the nematic LC-CNT composites has been reported by Chen et al. [24]. The authors stated that, for the lower transient current, the LC-CNT hybrid system has the ability to decrease the moving-ion density; and subsequently, the suppression of the undesired field screening takes place, leading to a reduced driving voltage. CNT-LC composites have also been utilized as microfluidic sensors, and lubricants due to their boundary layer rheological properties. Qiao et al. [25] have investigated the boundary layer and bulk viscosities for CNT-doped 5CB system. The authors have disclosed the existence of electroviscous effects on the boundary layer viscosity in the nematic and isotropic phases. Besides, the effect of CNTs on the dielectric and electro-optical properties has also been investigated. Gupta et al. [26] have described the influence of single-walled carbon nanotube (SWCNT) on ferroelectric LC; whereas, Malik et al. [27] have reported that the presence of multi-walled carbon nanotube (MWCNT) decreases the nematic–isotropic phase transition temperature (T_{NI}) and could enhance the response time by $\sim 80\%$ along with an improvement in the contrast ratio (CR) and lower threshold voltage. A series of papers by Basu et al. has provided a comprehensive overview on LC-CNT composites describing various aspects like nematic anchoring on CNT [16], orientational coupling [15], field induced nematic switching [28], electroclinic effect in achiral LC [29] and dielectric response as a function of an externally applied alternating field [30]. CNT-doped LC systems have been extensively studied by many other researches for the fundamental and technical applications. The ionic transport and screening in nematics with the addition of CNTs is an important field of scientific research that requires more attention; nevertheless, few attempts have already been mentioned in the literature [17,31]. This field requires more serious and systematic investigation as this fundamental aspect is essentially required for electro-optical devices.

Herein, we investigate the dielectric and electro-optical properties of a commercially available nematic mixture, namely E7, and their composites with different concentrations of multi-walled carbon nanotubes (MWCNTs). The dielectric parameters such as dielectric permittivity, anisotropy and splay elastic constant have been calculated from dielectric spectroscopic measurements. This investigation has revealed that up to a certain concentration, CNTs act as an ion catcher with higher ion trapping efficiency. Therefore, LC-CNT composites yield lesser free ions, leading to an enhancement in the dielectric anisotropy, decrease in the rotational viscosity and hence a faster electro-optical response in the composite system. The threshold limit of CNT concentration in composites has been also optimized after which the LC-CNT composite system renders slower switching. This investigation confers its utility for many fast-responsive electro-optical devices. The improvement in T_{NI} , dielectric anisotropy, electro-optical response time, birefringence, order parameter with varying concentrations of MWCNTs have been exhaustively studied and discussed.

2. Materials and Methods

The nematic LC namely E7 (Merck@ KGaA, Darmstadt, Germany, $T_{NI} = 60.5\text{ }^{\circ}\text{C}$) has been used in the present investigation (CAS No. 40817-08-1). This compound is basically a mixture of different LC monomers as follows: 5CB (51%), 7CB (25%), 8OCB (16%), and

7CT (8%) (Figure 1a). The E7 LC mixture exhibits a positive dielectric anisotropy ($\Delta\epsilon$) of 14.1, birefringence (Δn) of 0.22, nematic-isotropic phase transition temperature (T_{NI}) of 60.5 °C, rotational viscosity (γ) of 232.6 mPas, elastic constants K_{11} , K_{22} , and K_{33} values of 11.1, 5.9, and 17.1 pN, respectively, at 20 °C. A highly purified MWCNTs (impurity <5% Metal Oxide) were obtained from Sigma-Aldrich, St. Louis, MO, USA (CAS No. 308068-56-6) and had average diameter of 9.5 nm, inner diameter of 0.5–1 nm and an average length of 1.5 μm (Figure 1b). The LC-CNT composites were prepared by dispersing the MWCNT powder directly into the LC without any solvents; then the mixture was ultrasonically stirred for 30 min at room temperature (RT) in the isotropic phase. Then, 5 μm -thick cells, composed of two indium tin oxide (ITO) glass substrates, were constructed. The detailed process of sample cell fabrication could be obtained in our previous articles [10,32]. The cell thickness was estimated via the optical interferometry and found to be $\sim 5.3 \pm 0.05 \mu\text{m}$. The CNT concentration was set to 0.001, 0.005, 0.010 and 0.050 wt%. The LC mixtures were heated above the isotropic temperature to fill in the empty cells via capillary action and successively cooled down to the room temperature. Notably, the selection of cell thickness and length of CNT is very important because a high electric field across the CNT can cause a resistance blow-up effect [33]. Hence, in the present investigation, we have chosen MWCNTs exhibiting an average length of 1.5 μm , which is much smaller than the cell gap ($\sim 5.3 \mu\text{m}$) so that the LC cells could not short in the vertical configuration.

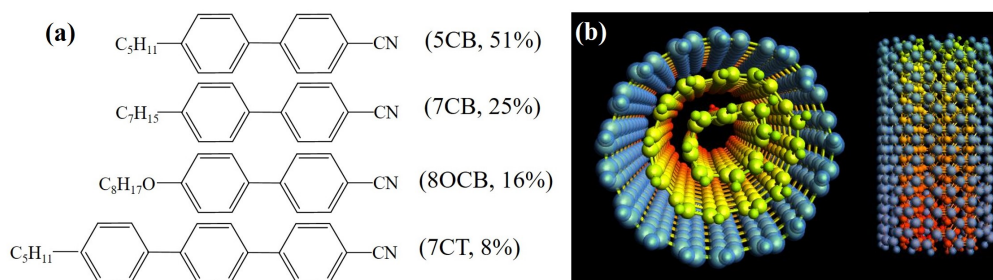


Figure 1. (a) represents the wt% constituents of the different monomers in the E7 LC mixture; whereas, (b) depicts the schematic of top and front views of MWCNTs (designed via Avogadro software [34]).

Various instruments and experimental techniques have been employed to consummate this investigation. Polarized optical microscope (DM EP, LEICA, Wetzlar, Germany) integrated with temperature controller (T95-PE, Linkam, Epsom, UK) was used to record the optical texture and to observe T_{NI} of the pure E7 and LC-MWCNT composites. The transmission spectra with the variation of wavelength was recorded using computer operated commercial software ISM-Lux by Isuzu Optics corp. Taiwan, integrated with a white light source. The response time was calculated by using an optical switching technique of the pure E7 and LC-MWCNT composites at room temperature (RT). Experimental setup and measurement techniques for voltage dependent transmission curve (V-T curve) and response time have already been reported in our previously published articles [10,32]. Crystal rotation method [35] was used to calculate the pre-tilt angles of the homogeneously (HA or ECB) and vertically aligned (VA) LC cells filled with the pure E7 and LC-MWCNT composites. The polar anchoring energy coefficients, W_{polar} , of the MWCNT-doped LC cells were calculated by using the high electric field techniques [36]. The values of pre-tilt angles and polar anchoring energy coefficients are listed in Table 1. The W_{polar} of MWCNT-doped LC cells is slightly increased as compared to the pristine E7. The dielectric spectra of the pure E7 and LC-MWCNT composites in the HA and VA configuration were measured using a LCR meter (Hioki 3532-50, Tokyo, Japan) with an applied alternating field of 0.01 V/ μm in the frequency regime of 42 Hz to 5.5 MHz to obtain the real and imaginary parts of complex dielectric permittivity. The Δn of the LCs was determined by using the phase retardation technique [32,37].

Table 1. The anchoring energy and pre-tilt angles in the pure E7 and its mixtures having different MWCNTs proportions.

MWCNTs wt% /Parameters	0 wt%	0.001 wt%	0.005 wt%	0.010 wt%	0.050 wt%
W_{polar} (10^{-4} J/m ²)	1.20	1.32	1.46	1.57	1.72
Pretilt in HA cell (degree)	2.55	2.42	2.36	2.16	2.00
Pretilt in VA cell (degree)	88.40	88.52	88.66	88.76	88.96

3. Results and Discussion

Figure 2 shows the polarized optical micrographs (POMs) of the pristine E7 LC and its mixtures exhibiting various concentrations of MWCNTs. In the POMs, rubbing direction was at 45° from the transmission axis of the polarizer. Figure 2a–e represent the bright states of the pristine E7 LC and their composites having 0.001, 0.005, 0.010 and 0.050 wt% concentrations of MWCNTs. It is noticed that the dispersion of MWCNTs has not affected the dark state of the E7 molecules; therefore, only a single dark state image, corresponding to the pristine E7 LC, has been depicted in Figure 2f. The homogeneous dispersion of MWCNTs in the E7 LC is evident from POMs. Any visible agglomerations or significant defects have not been observed. The uniformity of POM color in the entire bright state has also confirmed that the LC molecules are uniformly aligned in the nematic matrix of the E7 LC [37–41]. However, the dispersion of MWCNTs in the E7 LC into different concentrations leads to the change in color of POMs, which is associated to the change in refractive index and/or birefringence (Δn) as reported previously [42–44]. Besides, all the POM images have also been processed by ImageJ software to analyze the uniformity of color within a POM image. An intensity of ~ 7 a.u. has been obtained via this processing, which further confirms that the LC molecules are homogeneously oriented towards long molecular direction in the cells.

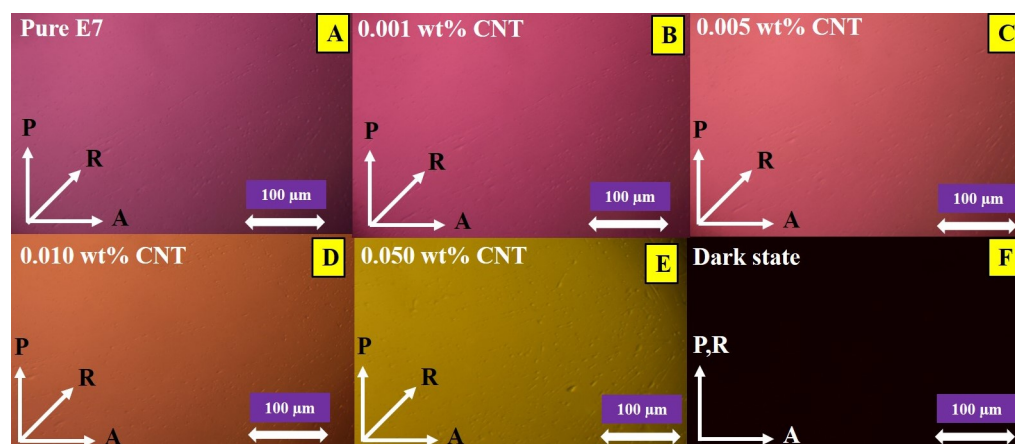
**Figure 2.** Bright state polarized optical micrographs (POMs) of (A) pristine E7 LC and (B) 0.001, (C) 0.005, (D) 0.010 and (E) 0.050 wt% MWCNTs dispersed E7 system. (F) represents the the dark state POM of the pristine E7 LC.

Figure 3 illustrates the “International Commission on Illumination (CIE)” chromato-graphic diagram and corresponding ‘x’ and ‘y’ coordinates are tabulated in Table 2, which represents the stimuli-induced color changes. The luminescence properties of the host E7 LC indicate that the intensity and luminescence color remain at the same position with increasing MWCNTs concentrations. This indicates that the MWCNTs dispersion in the E7 LC does not cause any color shifts in the LC cell despite having the absorbance for shorter wavelengths.

Table 2. CIE color coordinates (x,y) of MWCNTs doped E7 LC at room temperature.

MWCNTs wt%	x	y
Light source	0.4302	0.4206
Empty Cell	0.4612	0.4266
Pure E7	0.4597	0.4279
0.001 wt%	0.4599	0.4277
0.005 wt%	0.4594	0.4272
0.010 wt%	0.4593	0.4278
0.050 wt%	0.4593	0.4275

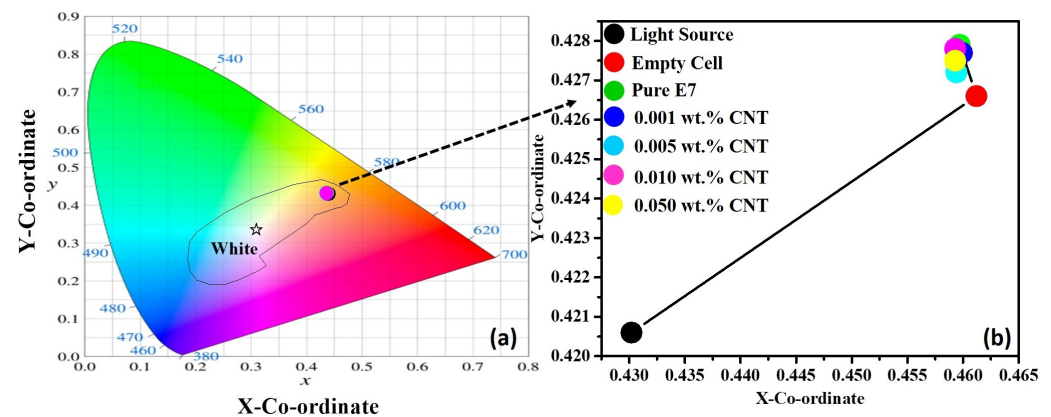
**Figure 3.** (a) CIE color chromaticity diagram and (b) CIE chromatographic coordinates of the pristine E7 LC and its composites with MWCNTs.

Figure 4 shows the room temperature (RT) V-T curves of the pristine and MWCNT-doped LC cells. No significant shift in V-T curves has been observed with increasing MWCNT concentrations, indicating that the petty amount of MWCNT dispersion does not affect the threshold voltage (V_{th}) and operation voltage (V_{op}) significantly. For the small applied field, the maximum transmission via E7 LC has been slightly reduced after the addition of MWCNTs, which might be attributed to the enhanced scattering of light and/or change in refractive index. Four different techniques have been used to analyze the V_{th} :

1. By V-T curve: V_{th} is defined as the voltage corresponding to which initial transmission of the V-T curve starts changing; however, this method is not so accurate as one can be confused between the V_{th} and distortion of transmitted light.
2. By phase curve: To define the V_{th} for MWCNT-doped LC composites, the V-T curves were transferred to voltage-dependent phase retardations in which V_{th} is described as the voltage required for the change in phase retardation from 100% to 90% of maximum value.
3. By POM image: The V_{th} is determined via POMs of the MWCNT-doped LC cells recorded at different voltages. The V_{th} is termed to be a particular voltage at which we observe a color change in POM. This color change evinces distortions in the LC cell.
4. By C-V curve: The V_{th} via C-V curves in MWCNT doped homogeneously aligned LC cells is defined as the voltage at which capacitance begins to increase. Among all four techniques, we have observed approximately the same value of V_{th} (~ 0.96 Volts) for the pure E7 LC and LC-MWCNT composites at RT.

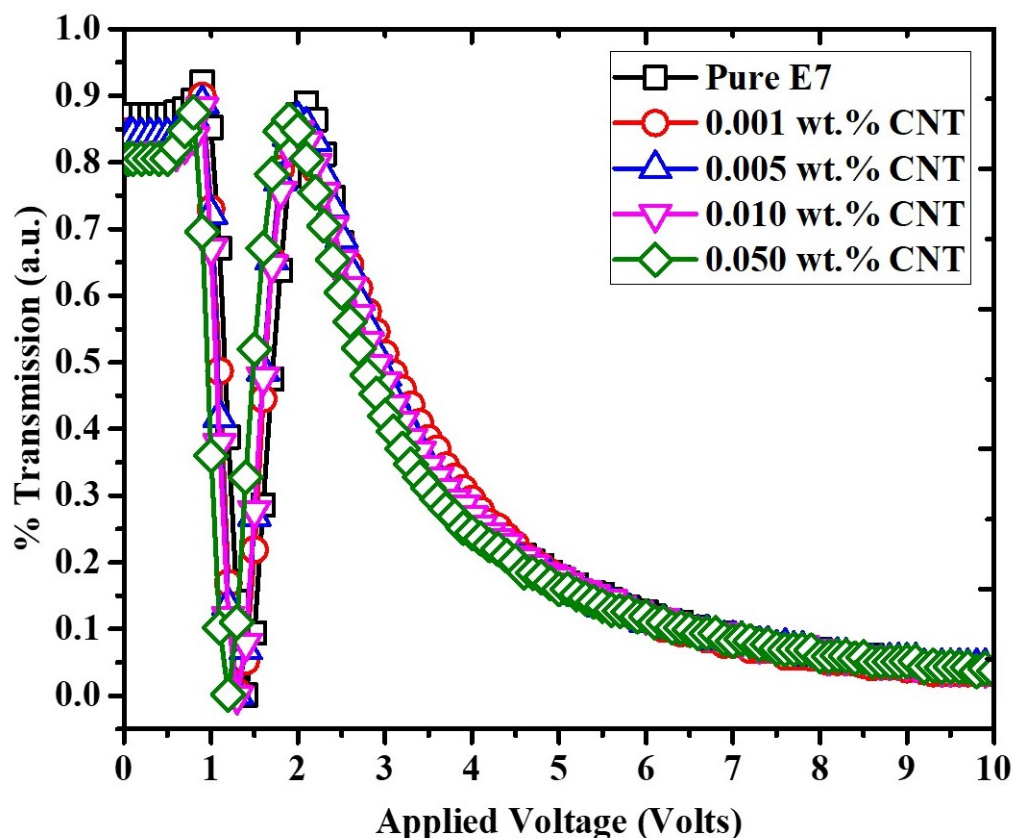


Figure 4. Variation of transmittance as a function of applied voltage (V-T curves) of the pristine E7 LC and its composites with different concentration of MWCNTs at room temperature (RT).

Contrast ratio (CR) is also an important parameter for an electro-optical display device. It is defined as: $CR = T_{on}/T_{off}$; where, T_{on} is maximum transmission and T_{off} is the minimum transmission of the pure E7 and MWCNT doped homogeneously aligned LC cells [41]. The calculation of CR has been done by processing the bright (on-state) and dark (off-state) states POMs using ImageJ software. Carefully taking the same scale of bright and dark state textures, we have calculated the average value of T_{on} and T_{off} of the pure E7 and MWCNT composites; which in turn gives the value of CR. In general, the contrast ratio of LCs could be enhanced by adding a guest material via refractive index matching [45]. LC/polymer-dispersed systems are somehow better for enhancing the CR [46]; however, in the present investigation, we have observed a reduced CR for the LC/MWCNTs composites due to the scattering of transmitted light from the MWCNTs and refractive index mismatching. On the other hand, ferroelectric LCs could render an enhanced CR with the addition of MWCNTs by enhancing the alignment [47]. The calculated values of V_{th} , V_{op} , and CR are listed in Table 3.

Table 3. Calculated values of threshold voltage (V_{th}), operating voltage (V_{op}), and contrast ratio (CR) of homogeneously aligned LC cells with the variation of MWCNTs concentrations at RT.

MWCNTs wt%	V_{th} (in V)	V_{op} (in V)	CR
Pure E7	0.96	2.01	27.25
0.001 wt%	0.96	2.01	25.88
0.005 wt%	0.96	2.00	24.68
0.010 wt%	0.96	2.00	23.83
0.050 wt%	0.96	2.00	22.75

The low-frequency dielectric properties of the E7 LC and its composites with different concentrations of MWCNTs are plotted in Figure 5. These properties have been analyzed using the Uemura model which can be represented as [48,49]:

$$\epsilon'(f) = A \times f^{-3/2} + B \quad (1)$$

and

$$\epsilon''(f) = C \times f^{-1} \quad (2)$$

where, $A = \frac{2nq^2D^{3/2}}{\epsilon_0\sqrt{\pi}dk_B T}$; $B = \epsilon_\infty$; and $C = \frac{2nq^2D}{\epsilon_0k_B T}$

Using Equations (1) and (2), the diffusion coefficient (D) can be calculated as:

$$D = \frac{2nA^2\pi \cdot d^2}{C^2} \quad (3)$$

The ion concentration, n , can be determined using the following relation:

$$n = \frac{C\epsilon_0k_B T}{2q^2D} \quad (4)$$

where, n is the ionic concentration, D is the diffusion constant of the ions, q is the electronic charge, k_B is the Boltzmann constant, T is an absolute temperature and d is the thickness of the LC sample holder. The Equations (1) and (2) do not describe the formation of electric double layer (EDL) however; the effect of space charge polarization can be explained using these equations. The EDL may strongly be dependent on the adsorption and desorption efficiencies of the impurity ions [50]. Here, the study of dielectric parameters is confined within the range 50 Hz to 1 kHz. DC conductivity can be represented in terms of diffusion constant and ionic concentration as: $\sigma_{dc} = nq^2D/k_B T$; whereas, AC conductivity is associated to dielectric loss as follows: $\sigma_{ac} = \epsilon_0\omega\epsilon''$. In general, LCs contain a significant amount of free ions. The ionic presence increases the rotational viscosity by slackening the response of the nematic director under the application of an external field. The MWCNTs act as barricades for ions with a high ion-trapping constant; consequently, the ions are trapped at the adsorbing sites of MWCNTs. Thus, the suspension of an adequate amount of MWCNTs in the LC medium lowers the free ion concentration and subsequently, decreases the rotational viscosity in the composites. The combined effect of enhanced dielectric anisotropy and lowered rotational viscosity of the E7 LC/MWCNTs composite system render a faster molecular response with the applied electric field, which could be used to develop the fast-responding LCDs. In the present study, we have also optimized the threshold limit of MWCNT concentration (0.05 wt%) above which the composite system gets perturbed and MWCNTs start aggregating. At this stage, additional generation of ions takes place and ion-trapping is no longer valid. Besides, a decreased birefringence and lower order parameter of the LC system would be achieved. In this investigation, we found the best results for 0.05 wt% of MWCNTs, which are listed in Table 4.

Table 4. The fitted values of the constants A, B and C and corresponding calculated values of ionic concentration (n), diffusion constant (D), dc conductivity (σ_{dc}) and mobility of ions (μ) of the pure and MWCNTs dispersed E7.

MWCNTs wt%	A	B	C	n ($\times 10^{19} \text{ m}^{-3}$)	D ($\times 10^{-10} \text{ m}^2/\text{s}$)	σ_{dc} ($\times 10^{-9} \text{ S/m}$)	μ ($\times 10^{-9} \text{ m}^2/\text{V}\cdot\text{s}$)
Pure E7	1962.41	5.53	1803.37	1.28	1.01	7.98	3.89
0.001 wt%	2002.23	5.45	1768.59	1.16	1.09	7.83	4.21
0.005 wt%	3653.13	5.51	2393.83	0.866	1.98	10.6	7.64
0.010 wt%	4514.48	5.18	2747.96	0.858	2.29	12.2	8.86
0.050 wt%	5301.61	5.04	3040.79	0.843	2.58	13.5	9.97

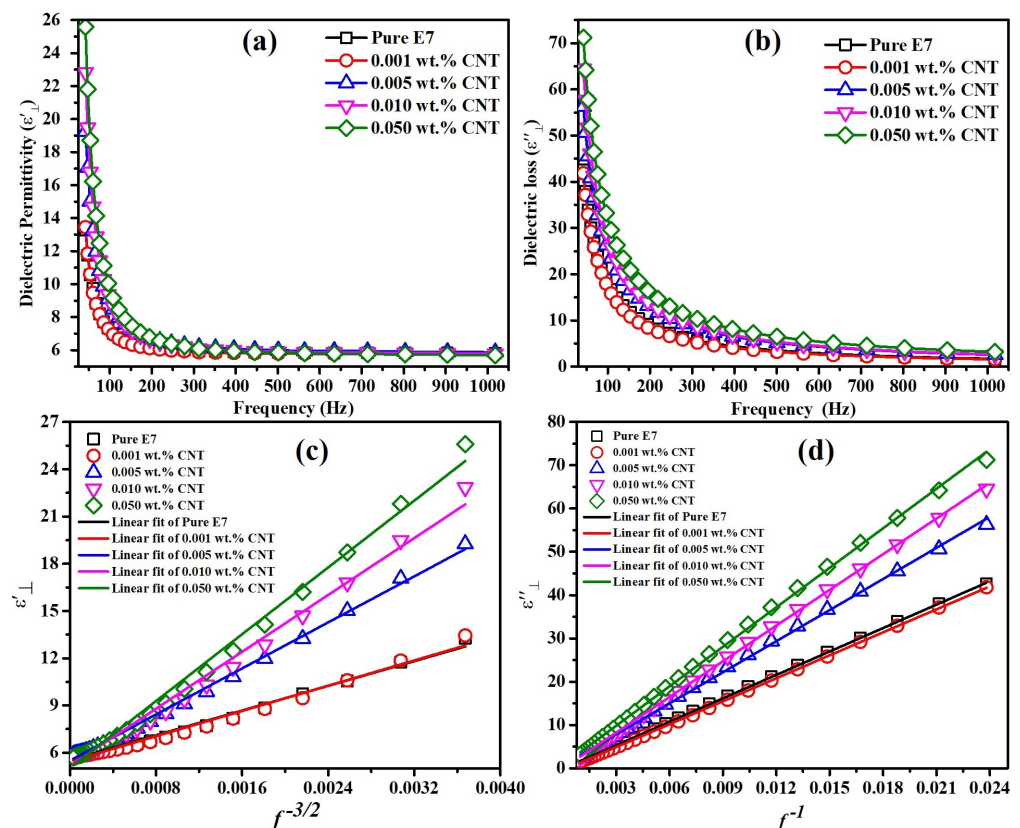


Figure 5. (a) Dielectric permittivity and (b) dielectric loss as a function of the frequency for the pure E7 LC and its composites with varying concentrations of MWCNTs. (c,d) represent the linear fitting of the experimental data of the corresponding dielectric permittivity and dielectric loss of the E7 LC at different doping concentrations of MWCNTs at RT.

Figure 6 shows the dielectric spectra of homogeneously (HA) and vertically (VA)-aligned MWCNTs dispersed E7 LC cells. Figures 6a,c show the variation of perpendicular and parallel components of dielectric permittivities (ϵ'_{\perp} and ϵ'_{\parallel}) as a function of frequency for the pure E7 and MWCNT doped E7 at RT. Interestingly, the MWCNT doping decreases the dielectric permittivity of HA cells (ϵ'_{\perp}) and increases the dielectric permittivity of VA cells (ϵ'_{\parallel}). Consequently, the dielectric anisotropy ($\Delta\epsilon = \epsilon'_{\parallel} - \epsilon'_{\perp}$) found to be increased with increasing MWCNT concentration.

For an effective dispersion of MWCNTs in LCs, a polar LC is required as MWCNTs render strong dipole–dipole interaction with it due to their greater polarizability along the CNT axis. The E7 LC/MWCNTs composites follow the same criteria. LCs exhibiting a large dipole moment depict strong interactions between the LC molecules and MWCNTs. It consists of a negative effect too. Very strong interactions lead to anti-parallel orientations which restrict the possibility of good dispersion of CNTs in the host LCs. Therefore, the optimization of a threshold concentration of CNTs in the LC media is an important factor; henceforth, a LC material with a moderate dipole moment is opted to take as a host for making the composites with CNTs. A particular orientation of CNTs can be obtained by inflicting the self-organization of LC molecules. The intrinsic orientation of LCs can also be tuned with CNTs. The free energy of the LC-CNT composite would be minimum, when CNTs are aligned along the director (see Supplementary Figure S1). Besides these factors, π - π stacking is another parameter that is vital in deciding the strong interaction between CNTs and LC molecules. A strong anchoring energy, due to π - π stacking of phenyl parts of the LC and carbon ring of MWCNTs, results in an increase in the $\Delta\epsilon$ (listed in Table 2) for the composite system; indicating a remarkable enhancement in the orientational order parameter. Herein, only very small concentration (≤ 0.05 wt%) of MWCNTs in the LCs is found to be well dispersed; however, higher concentrations

(>0.05 wt%) cause the formation of agglomeration because of strong van der Waals forces (in case of direct dispersion, i.e., without any organic solvent).

Figure 6d shows that the peak frequency, f_p , close to the 10^6 Hz, for the VA cells has slightly decreased and shifted towards the higher frequency region with the increasing MWCNTs concentrations. This relaxation mode is analogous to the reorientation of LC molecules around the short axis. The relaxation time (τ_{\parallel}) of LC molecules belongs to the f_p of the dielectric loss, as shown in the following equation:

$$\tau_{\parallel} = \frac{1}{2\pi f_p} \quad (5)$$

The addition of MWCNTs provides a noteworthy shift in the f_p of dielectric loss for the LC mixtures; and hence, decreases the relaxation time of the LC molecules. Further, Meier and Saupe indicated that the relaxation time, τ , in the vertically aligned cell, is associated to the potential barrier parameter, η , as follows [51]:

$$\eta = \frac{b}{RT} \quad (6)$$

where, b is the rotation barrier height of the flip-flops of the molecules around the axis, R is the gas constant, and T is the temperature. The barrier height prevents the molecular rotations; hence, the relaxation time (τ) becomes slower in comparison to a situation at $b = 0$. A retardation factor (g) is introduced, of which the (η) represents a proportionality with the relaxation time (τ) as follows [52]:

$$g = \frac{\tau}{\tau_0} = \frac{\exp(\eta) - 1}{\eta} \quad (7)$$

where, τ_0 is termed to a hypothetical state with $b = 0$.

As shown in Figure 7a,b, the addition of MWCNTs remarkably decreases the τ along with a decrease in the rotation barrier height around the short axes of the LCs. Subsequently, the associated rotational viscosity, γ , for the LC-MWCNTs composites also decreases [53]. The reduction in rotational viscosity for the composite results in a faster molecular response as a function of MWCNT concentrations. One should remember that the exact value of relaxation frequencies is always higher than those measured in the LC cells due to the hampering of cell relaxation [54,55]. The exact values of relaxation frequencies have not been evaluated due to the absence of information about the accurate ITO resistance and inductance of the wire; nevertheless, the influence of MWCNTs dispersion on the different parameters of the E7 LC could be explained.

Figure 7a,b represent the variation of rotational viscosity and dynamic response, respectively, for the pure E7 with different MWCNTs concentrations. The theoretical and experimental analysis indicates that the rotational viscosity of the E7 LC has been decreased with the addition of MWCNTs (~35% for 0.05 wt%). Importantly, we found that the relaxation processes are not only governed by the rotational viscosity, but also affected by concentration of ionic impurities. Our observations reveal that an appropriate amount of MWCNTs (from 0.005 to 0.05 wt%) significantly reduces the ion concentration (~34.3% for 0.05 wt%) via the ion trapping mechanism. The diminished ionic concentration offers a reduced field-screening effect. The reduced ionic concentration suppresses the image-sticking in the absence of an externally applied voltage resulting in the faster relaxation process.

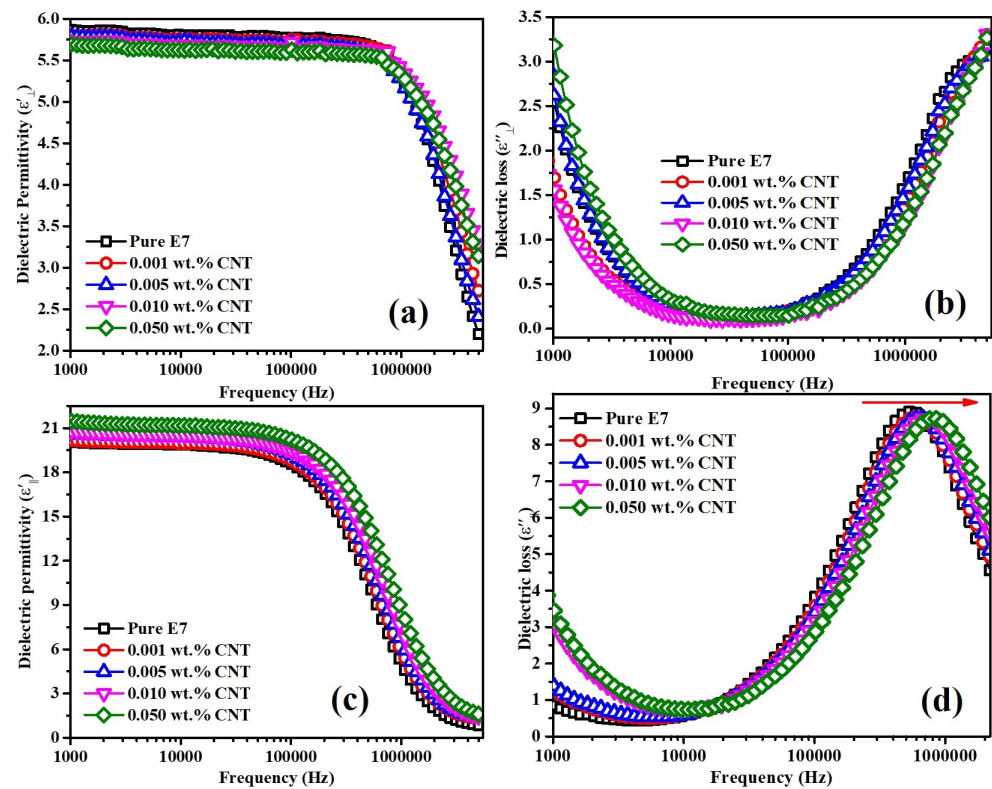


Figure 6. Room temperature dielectric spectra of the E7 LC and its composites with different concentrations of MWCNTs. (a) Dielectric permittivity and (b) dielectric loss of the homogeneously aligned LC cells; whereas, (c,d) represent the dielectric permittivity and dielectric loss of the vertically aligned LC cells, respectively.

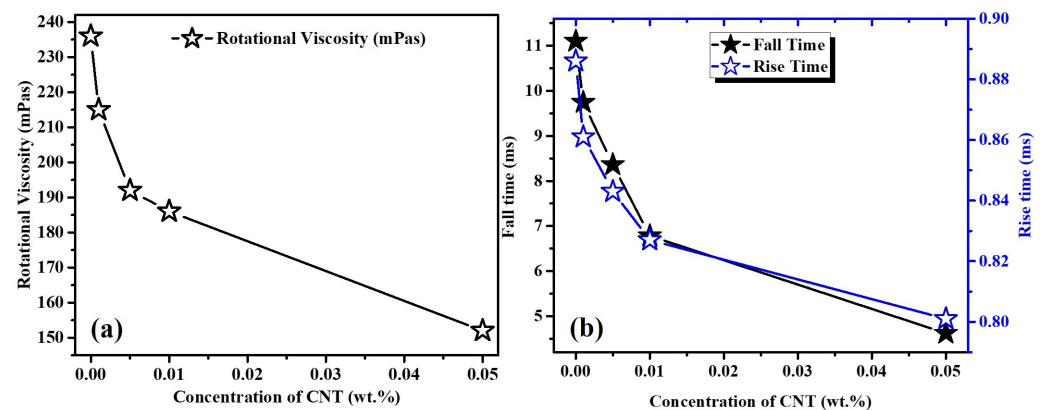


Figure 7. (a) Variation of rotational viscosity and (b) dynamic response of the pure E7 with different MWCNTs concentration.

Figure 7b shows the field-induced switching response for the pure E7 LC and LC-MWCNT composites at various doping concentrations. The dynamic response has been measured at a voltage higher than the threshold switching voltage. The rise and fall times could be described as the time needed for change in transmission from 90% to 10% and 10% to 90%, respectively, with respect to the maximum transmission when the applied voltage on the LC cell is turned on from 2 to 10 V (or turned off from 10 to 2 V). In general, the rise time (electric torque-driven reorientation) is always smaller as compared to the fall time (reorientation under free relaxation). The rise times of the pure E7 and MWCNT-doped LC cells have been found to be ~ 0.886 ms, 0.861 ms, 0.843 ms, 0.827 ms and 0.801 ms at RT, due to the different turn-on voltages (driving voltage) ranging from 2.12 V to 1.89 V. Notably, the fall time of MWCNT-doped LC cell decreases with increasing MWCNT concentration,

which is attributed to the decreased value of γ for the LC-MWCNTs composites. Interestingly, the 0.05 wt% MWCNT-doped LC cell emerges the $\sim 58\%$ faster fall time as compared to the pure E7 LC at RT. If the $V_{app} \gg V_{th}$, the relationships between fall time (τ_{off}), rise time (τ_{on}), V_{th} , and γ can be written as [42]:

$$\tau_o = \frac{\gamma d^2}{K_{11} \cdot \pi^2} \quad (8)$$

$$\tau_{on} = \frac{\tau_o}{|(V_{app}/V_{th})^2 - 1|} \quad (9)$$

$$\tau_{off} = \frac{\tau_o}{|(V_{bias}/V_{th})^2 - 1|} \quad (10)$$

where τ_o is the relaxation time when the LC cell is turned off from V_{app} to slightly higher than V_{th} , K_{11} is splay elastic constant, V_{bias} is the bias voltage, and d is known to be cell thickness.

The presence of MWCNTs in the E7 LC has significantly decreased the τ_{off} due to the reduced γ and V_{th} . Notably, MWCNT doping decreases τ_{off} and K_{11} and hence γ , which confirms the conjecture of Equations (8) and (10). It is really interesting to explore the reason that why the presence of MWCNTs remarkably reduces the switching time of nematic molecules. For a planar cell, the response of nematic director under an external applied field could be understood by Equations (8)–(10). These equations express the field-induced nematic switching, which is not only the optical response. This is the time taken by the nematic director to switch between planar to homeotropic orientations. Since an optical response principally arises due to the rotation of the director in the presence of an applied field, we can write $\tau_{on} \propto \tau_o$, by overlooking the cell backflow. Hence, from Equations (8)–(10), for a constant d , V_{app} and V_{th} , the faster response could be obtained for LC-MWCNT composite system with a reduced γ ($\sim 35\%$), enhanced $\Delta\epsilon$ ($\sim 3.5\%$), and reduced K_{11} ($\sim 24\%$). We have additionally performed experiments to find out γ and $\Delta\epsilon$ for the pure E7 LC and LC-MWCNTs composites. Table 5 shows that MWCNT dispersion has increased the T_{NI} of the LC mixture, measured by POM from N \rightarrow Iso (nematic to isotropic) phase with a heating rate of $0.25 \text{ }^\circ\text{C}/\text{min}$. Moreover, MWCNT dispersion in the E7 LC has increased the order parameter S and Δn of composites following to Equations (1) and (5) [56,57].

Table 5. MWCNTs concentration-dependent birefringence (Δn), nematic–isotropic temperature (T_{NI}), and estimated orientational order parameter (S) of the pure E7 LC and its composites at RT.

MWCNTs wt%	Δn	T_{NI} (in $^\circ\text{C}$)	S
Pure E7	0.216	60.50	0.583
0.001 wt%	0.219	61.50	0.592
0.005 wt%	0.226	63.00	0.611
0.010 wt%	0.232	65.00	0.627
0.050 wt%	0.248	66.50	0.670

The concentration dependence of the birefringence (Δn), nematic–isotropic temperature (T_{NI}), and estimated second order orientational order parameter (S) of the pure LC composites are listed in Table 5. The birefringence increases with the dispersion of MWCNT in the E7 LC (up to 0.05 wt%). For 0.001, 0.005, 0.01 and 0.05 wt%, we have observed the increment of 1.38, 4.63, 7.1 and 14.82 %, respectively. This enhancement of birefringence can be attributed to the increased T_{NI} , and S of LC-MWCNT composites.

Haller’s extrapolation technique was adopted to calculate the orientational order parameter [58–60].

$$\Delta n = \Delta n_o \left(1 - \frac{T}{T^*}\right)^\beta \quad (11)$$

where, Δn_0 , T^* and β are the adjustable parameters, which are listed in Table 5. Δn is the temperature dependent birefringence, Δn_0 is the extrapolated birefringence in the perfectly ordered state (i.e., $T = 0$ K), T^* is the temperature which is about 1–4 K higher than the isotropic temperature (T_{NI}) and b is the critical exponent value close to 0.25, which depends on the molecular structure of the material. Equation (11) holds its validity if T is sufficiently smaller than T_{NI} [61]. This method allows us to evaluate Δn at absolute zero temperature and to determine Δn_0 .

The variation of order parameter (S) can be presented as:

$$S = \left(1 - \frac{T}{T_{NI}}\right)^\beta \quad (12)$$

Equation (12) is only valid when, $T \ll T_{NI}$ [48,49]. Though, MWCNT dispersion has significantly increased the T_{NI} (measured by POM) and hence the associated Δn and S of the pure and MWCNT doped LC have also been increased according to Equations (11) and (12) [56,57]. The birefringence Δn is linked with the order parameter (S) of LC as follows:

$$S = \frac{\Delta n}{\Delta n_0} \quad (13)$$

Here, Δn is the birefringence at a particular temperature and Δn_0 is the birefringence at the absolute zero temperature for the perfect ordering as assumed in the Haller's approximation for the order parameter S . Our investigation reveals that the value of Δn_0 is about 0.37 for $\lambda = 633$ nm at RT, which is in accordance with the available literature [62–64]. In the LC-MWCNT composite system, the inherent order of the LC can be transferred to MWCNTs. The anisotropic elastic forces of the LC lead to a situation at which the minimum free energy for the MWCNT-LC matrix is reached for a configuration where the MWCNTs align along the director of LC molecules. The LC-MWCNTs coupling renders a positive impact on the LC's orientational threshold and elasticity, which permits the director of nematic molecules to orient quickly along with MWCNTs [65,66]. If the MWCNTs are well dispersed in the nematic LC, the anisotropic elastic forces try to minimize the free energy of the system. The free energy of the MWCNT-LC matrix is minimized when the MWCNTs align along the director of E7 LC (i.e., $\alpha = 0, \pi, 2\pi$, etc.); where, α is the angle between the long axis of MWCNTs and director, \bar{n} , of the LCs [38]. As anticipated, the order parameter increases with increasing MWCNT's concentration. The increment in the order parameter is possibly due to the enhanced anchoring effect by π - π interaction between the LC molecules and MWCNTs. It is also worth mentioning that the T_{NI} of the LC mixture has been enhanced by the dispersion of MWCNTs, which indicates the improvement of nematic order and broad nematic range [15,67]. Since MWCNTs used in the present investigation are not ferromagnetic; therefore, the additional ordering must not be because of the electronic coupling between the permanent dipole moment of MWCNT and the dielectric anisotropy of the LC molecules [68]. Hence, the enhancement in $\Delta\epsilon$ and subsequent improvement in S is attributed due to the anisotropic structure of MWCNTs and enhanced anchoring energy (since $\Delta\epsilon \propto S$). In the present investigation, the enhancement in the order parameter has been found to be 1.54%, 4.80%, 7.55% and 14.92% for the 0.001, 0.005, 0.01 and 0.05 wt% MWCNTs, respectively.

The elastic constants in the LC media characterize the elastic interactions between the LC molecules. When MWCNTs are dispersed in LCs, the elastic constant (K_{11}) also renders an interaction between the LC molecules and the MWCNT dopant [69]. For the LC-MWCNT composite, K_{11} can be roughly estimated by a well-known relation:

$$V_{th} = \pi \sqrt{\frac{K_{11}}{\epsilon_0 \Delta\epsilon}} \quad (14)$$

where, V_{th} is the reorientation threshold voltage for Fréedericksz transition. The K_{11} is estimated using the experimentally observed values of V_{th} and $\Delta\epsilon$ by putting it in Equation (14).

Notably, $K_{11} \propto V_{th}^2$ and $\Delta\epsilon$. Since the dispersion of MWCNTs does not significantly affect V_{th} , it is approximately constant ($V_{th}^{(LC+CNT)} \approx V_{th}^{LC}$), i.e., the increasing value of $\Delta\epsilon$ leads to an increased K_{11} for MWCNT dispersed composites; i.e., $K_{11}^{(LC+CNT)} > K_{11}^{LC}$. It is worth noting that, $\sqrt{K_{11}^{LC} / \Delta\epsilon^{LC}} \approx \sqrt{K_{11}^{LC+CNT} / \Delta\epsilon^{LC+CNT}} = 0.91$; which gives $K_{11}^{(LC+CNT)} = 1.11 K_{11}^{LC}$ for 0.05 wt% MWCNTs. Therefore, the surface anchoring seems to be accountable for the strong elastic interaction between the LC molecules and MWCNTs, which increases the elastic energy in the LC-MWCNT composites providing an increase in K_{11} .

4. Conclusions

In summary, a well-known nematic LC mixture namely E7 has been dispersed with MWCNTs into different concentrations ranging from 0.001 to 0.05 wt%. The dielectric and electro-optical investigations were carried out in the homogeneously and vertically aligned ITO cells. Due to the small dispersion concentration, MWCNTs have been well-dispersed into the nematic matrix, which was confirmed with POMs; however, the transmission via LC cells was found to be slightly reduced due to the scattering of light from the edges of MWCNTs. Within the dispersion limit, MWCNTs act like barricades for ionic impurities by reducing them up to $\sim 34.3\%$. The ionic screening leads to an enhanced $\Delta\epsilon$ and K_{11} for the LC-MWCNTs composites. Consequently, a drastic decrement in the rotational viscosity and hence an increase of about $\sim 60\%$ in electro-optical response has been noticed. Moreover, the dispersion of MWCNTs in the E7 LC also offered an enhancement about $\sim 15\%$ in the S and Δn due to the increased T_{NI} and anchoring energy via π - π electron stacking between the LC molecules and MWCNTs. The obtained results have demonstrated that the dispersion of a small amount of MWCNTs in the LC could significantly enhance the device parameters, which is useful for the development of futuristic electro-optical devices.

Supplementary Materials: The following are available online at <https://www.mdpi.com/article/10.3390/electronicmat2040032/s1>, Figure S1: Illustration of the E7 LC molecules/MWCNTs composite showing the minimum free energy condition when the MWCNTs are aligned along with the director.

Author Contributions: Conceptualization, writing—original draft preparation, B.P.S.; reviewing and editing, S.S.; supervision, visualization, R.M.; resources, methodology, K.K.P.; reviewing and supervision of all works in France and draft writing, D.P.S. and M.D. All authors have read and agreed to the published version of the manuscript.

Funding: The author B.P.S. is sincerely thankful for the INSPIRE-AORC Program of the Department of Science & Technology (DST), New Delhi [No. DST/INSPIRE Fellowship/2016/IF160572] for providing financial assistance in the form of INSPIRE Fellowship. Author R.M. is thankful to UGC for ‘MID CAREER AWARD’ [No.F.19-224/2018 (BSR)].

Institutional Review Board Statement: Not applicable.

Informed Consent Statement: Not applicable.

Data Availability Statement: The data presented in this study are available on request from the corresponding authors.

Acknowledgments: Authors are also thankful to the A.P.J. Abdul Kalam Centre for Innovation for the experimental facilities. Chi-Yen Huang and Che-Ju Hsu, National Changhua University of Education, Taiwan are sincerely acknowledged for providing the experimental facilities and valuable discussion. D.P.S. gratefully acknowledges the financial assistance provided by the UDSMM, ULCO. A. Hadj Sahraoui, Director UDSMM is highly acknowledged for their kind support.

Conflicts of Interest: The authors declare no conflict of interest. The funders had no role in the design of the study; in the collection, analyses, or interpretation of data; in the writing of the manuscript, or in the decision to publish the results.

References

1. Jain, K.; Klosner, M.; Zemel, M.; Raghunandan, S. Flexible Electronics and Displays: High-Resolution, Roll-to-Roll, Projection Lithography and Photoablation Processing Technologies for High-Throughput Production. *Proc. IEEE* **2005**, *93*, 1500–1510. [[CrossRef](#)]
2. Hsu, C.J.; Singh, B.P.; Antony, M.; Selvaraj, P.; Manohar, R.; Huang, C.Y. Liquid crystal lens with doping of rutile titanium dioxide nanoparticles. *Opt. Express* **2020**, *28*, 22856–22866. [[CrossRef](#)] [[PubMed](#)]
3. Driencourt, L.; Federspiel, F.; Kazazis, D.; Tseng, L.T.; Frantz, R.; Ekinci, Y.; Ferrini, R.; Gallinet, B. Electrically Tunable Multicolored Filter Using Birefringent Plasmonic Resonators and Liquid Crystals. *ACS Photonics* **2020**, *7*, 444–453. [[CrossRef](#)]
4. Chen, C.W.; Brigeman, A.N.; Ho, T.J.; Khoo, I.C. Normally transparent smart window based on electrically induced instability in dielectrically negative cholesteric liquid crystal. *Opt. Mater. Express* **2018**, *8*, 691–697. [[CrossRef](#)]
5. Zhang, Y.; Yang, X.; Zhan, Y.; Zhang, Y.; He, J.; Lv, P.; Yuan, D.; Hu, X.; Liu, D.; Broer, D.J.; et al. Electroconvection in Zwitterion-Doped Nematic Liquid Crystals and Application as Smart Windows. *Adv. Opt. Mater.* **2021**, *9*, 2001465. [[CrossRef](#)]
6. Wang, Z.; Xu, T.; Noel, A.; Chen, Y.C.; Liu, T. Applications of liquid crystals in biosensing. *Soft Matter* **2021**, *17*, 4675–4702. [[CrossRef](#)] [[PubMed](#)]
7. Christodoulou, C.G.; Tawk, Y.; Lane, S.A.; Erwin, S.R. Reconfigurable Antennas for Wireless and Space Applications. *Proc. IEEE* **2012**, *100*, 2250–2261. [[CrossRef](#)]
8. Carlton, R.J.; Hunter, J.T.; Miller, D.S.; Abbasi, R.; Mushenheim, P.C.; Tan, L.N.; Abbott, N.L. Chemical and biological sensing using liquid crystals. *Liq. Cryst. Rev.* **2013**, *1*, 29–51. [[CrossRef](#)]
9. Singh, D.P.; Gupta, S.K.; Yadav, S.P.; Sharma, P.K.; Pandey, A.C.; Manohar, R. Guest–host interaction in ferroelectric liquid crystal–nanoparticle composite system. *Bull. Mater. Sci.* **2014**, *37*, 511–518. [[CrossRef](#)]
10. Singh, B.P.; Huang, C.Y.; Singh, D.P.; Palani, P.; Duponchel, B.; Sah, M.; Manohar, R.; Pandey, K.K. The scientific duo of TiO₂ nanoparticles and nematic liquid crystal E204: Increased absorbance, photoluminescence quenching and improving response time for electro-optical devices. *J. Mol. Liq.* **2021**, *325*, 115130. [[CrossRef](#)]
11. Latypov, Z.Z.; Pozdnyakov, O.F. Determining conditions for the preparation of polymer films containing an ordered structure of carbon nanotubes and higher fullerenes. *Tech. Phys. Lett.* **2006**, *32*, 381–383. [[CrossRef](#)]
12. Mayer, A. Formulation in terms of normalized propagators of a charge-dipole model enabling the calculation of the polarization properties of fullerenes and carbon nanotubes. *Phys. Rev. B* **2007**, *75*, 045407. [[CrossRef](#)]
13. Macutkevic, J.; Seliuta, D.; Valusis, G.; Banyas, J.; Kuzhir, P.; Maksimenko, S.; Kuznetsov, V.; Moseenkov, S.; Shenderova, O.; Lambin, P. Dielectric properties of onion-like carbon based polymer films: Experiment and modeling. *Solid State Sci.* **2009**, *11*, 1828–1832. [[CrossRef](#)]
14. Sabirov, D.S. Polarizability as a landmark property for fullerene chemistry and materials science. *RSC Adv.* **2014**, *4*, 44996–45028. [[CrossRef](#)]
15. Basu, R.; Iannacchione, G.S. Orientational coupling enhancement in a carbon nanotube dispersed liquid crystal. *Phys. Rev. E* **2010**, *81*, 051705. [[CrossRef](#)] [[PubMed](#)]
16. Basu, R.; Iannacchione, G.S. Nematic anchoring on carbon nanotubes. *Appl. Phys. Lett.* **2009**, *95*, 173113. [[CrossRef](#)]
17. Rahman, M.; Lee, W. Scientific duo of carbon nanotubes and nematic liquid crystals. *J. Phys. D Appl. Phys.* **2009**, *42*, 063001. [[CrossRef](#)]
18. Moghadas, F.; Poursamad, J.B.; Sahrai, M.; Emdadi, M. Flexoelectric coefficients enhancement via doping carbon nanotubes in nematic liquid crystal host. *Eur. Phys. J. E* **2019**, *42*, 103. [[CrossRef](#)]
19. Petrov, D.A.; Skokov, P.K.; Zakhlevnykh, A.N.; Makarov, D.V. Magnetic segregation effect in liquid crystals doped with carbon nanotubes. *Beilstein J. Nanotechnol.* **2019**, *10*, 1464–1474. [[CrossRef](#)]
20. Garbovskiy, Y. Conventional and unconventional ionic phenomena in tunable soft materials made of liquid crystals and nanoparticles. *Nano Express* **2021**, *2*, 012004. [[CrossRef](#)]
21. Varshini, G.V.; Shankar Rao, D.S.; Mukherjee, P.K.; Krishna Prasad, S. Nanophase Segregation of Nanostructures: Induction of Smectic A and Re-Entrance in a Carbon Nanotube/Nematic Liquid Crystal Composite. *J. Phys. Chem. B* **2018**, *122*, 10774–10781. [[CrossRef](#)]
22. Dolgov, L.; Yaroshchuk, O.; Lebovka, M. Effect of Electro-Optical Memory in Liquid Crystals Doped with Carbon Nanotubes. *Mol. Cryst. Liq. Cryst.* **2008**, *496*, 212–229. [[CrossRef](#)]
23. Petrov, D.A.; Skokov, P.K.; Zakhlevnykh, A.N. Magnetic field induced orientational transitions in liquid crystals doped with carbon nanotubes. *Beilstein J. Nanotechnol.* **2017**, *8*, 2807–2817. [[CrossRef](#)] [[PubMed](#)]
24. Chen, H.Y.; Lee, W. Suppression of field screening in nematic liquid crystals by carbon nanotubes. *Appl. Phys. Lett.* **2006**, *88*, 222105. [[CrossRef](#)]
25. Qiao, X.; Zhang, X.; Guo, Y.; Yang, S.; Tian, Y.; Meng, Y. Boundary layer viscosity of CNT-doped liquid crystals: Effects of phase behavior. *Rheol. Acta* **2013**, *52*, 939–947. [[CrossRef](#)]
26. Gupta, S.K.; Kumar, A.; Srivastava, A.K.; Manohar, R. Modification in dielectric properties of SWCNT doped ferroelectric liquid crystals. *J. Non-Cryst. Solids* **2011**, *357*, 1822–1826. [[CrossRef](#)]
27. Malik, P.; Chaudhary, A.; Mehra, R.; Raina, K.K. Electro-optic, thermo-optic and dielectric responses of multiwalled carbon nanotube doped ferroelectric liquid crystal thin films. *J. Mol. Liq.* **2012**, *165*, 7–11. [[CrossRef](#)]
28. Basu, R. Effect of carbon nanotubes on the field-induced nematic switching. *Appl. Phys. Lett.* **2013**, *103*, 241906. [[CrossRef](#)]

29. Basu, R.; Petschek, R.G.; Rosenblatt, C. Nematic electroclinic effect in a carbon-nanotube-doped achiral liquid crystal. *Phys. Rev. E* **2011**, *83*, 041707. [[CrossRef](#)]
30. Basu, R.; Iannacchione, G.S. Dielectric response of multiwalled carbon nanotubes as a function of applied ac-electric fields. *J. Appl. Phys.* **2008**, *104*, 114107. [[CrossRef](#)]
31. Yadav, S.P.; Singh, S. Carbon nanotube dispersion in nematic liquid crystals: An overview. *Prog. Mater. Sci.* **2016**, *80*, 38–76. [[CrossRef](#)]
32. Singh, B.P.; Sikarwar, S.; Agrahari, K.; Tripathi, S.; Gangwar, R.K.; Manohar, R.; Pandey, K.K. Electro-optical characterization of a weakly polar liquid crystalline compound influenced polyvinyl pyrrolidone capped gold nanoparticles. *J. Mol. Liq.* **2021**, *325*, 115172. [[CrossRef](#)]
33. Arora, V.K.; Bhattacharyya, A. Cohesive band structure of carbon nanotubes for applications in quantum transport. *Nanoscale* **2013**, *5*, 10927–10935. [[CrossRef](#)] [[PubMed](#)]
34. Hanwell, M.D.; Curtis, D.E.; Lonie, D.C.; Vandermeersch, T.; Zurek, E.; Hutchison, G.R. Avogadro: An advanced semantic chemical editor, visualization, and analysis platform. *J. Cheminform.* **2012**, *4*, 17. [[CrossRef](#)] [[PubMed](#)]
35. Baur, G.; Wittwer, V.; Berreman, D.W. Determination of the tilt angles at surfaces of substrates in liquid crystal cells. *Phys. Lett. A* **1976**, *56*, 142–144. [[CrossRef](#)]
36. Nastishin, Y.A.; Polak, R.D.; Shiyanovskii, S.V.; Bodnar, V.H.; Lavrentovich, O.D. Nematic polar anchoring strength measured by electric field techniques. *J. Appl. Phys.* **1999**, *86*, 4199–4213. [[CrossRef](#)]
37. Singh, B.P.; Pathak, G.; Roy, A.; Hegde, G.; Tripathi, P.K.; Srivastava, A.; Manohar, R. Investigation of dielectric and electro-optical properties of nematic liquid crystal with the suspension of biowaste-based porous carbon nanoparticles. *Liq. Cryst.* **2019**, *46*, 1808–1820. [[CrossRef](#)]
38. Lagerwall, J.P.F.; Scalia, G. Carbon nanotubes in liquid crystals. *J. Mater. Chem.* **2008**, *18*, 2890–2898. [[CrossRef](#)]
39. Chang, C.; Zhao, Y.; Liu, Y.; An, L. Liquid crystallinity of carbon nanotubes. *RSC Adv.* **2018**, *8*, 15780–15795. [[CrossRef](#)]
40. Vimal, T.; Singh, D.; Gupta, S.; Pandey, S.; Agrahari, K.; Manohar, R. Thermal and optical study of semiconducting CNTs-doped nematic liquid crystalline material. *Phase Transit.* **2016**, *89*, 632–642. [[CrossRef](#)]
41. Raina, K.; Kumar, P.; Malik, P. Morphological control and polarization switching in polymer dispersed liquid crystal materials and devices. *Bull. Mater. Sci.* **2006**, *29*, 599–603. [[CrossRef](#)]
42. Singh, D.P.; Visvanathan, R.; Duncan, A.E.; Duponchel, B.; Boussoualem, Y.; Kumar, S.; Clark, N.A.; Blach, J.F.; Douali, R.; Daoudi, A. CdSe quantum dots in chiral smectic C matrix: Experimental evidence of smectic layer distortion by small and wide angle X-ray scattering and subsequent effect on electro-optical parameters. *Liq. Cryst.* **2018**. [[CrossRef](#)]
43. Singh, D.P.; Duponchel, B.; Boussoualem, Y.; Agrahari, K.; Manohar, R.; Kumar, V.; Pasricha, R.; Pujar, G.H.; Inamdar, S.R.; Douali, R.; et al. Dual Photoluminescence and Charge Transport in alkoxy biphenyl benzoate ferroelectric liquid crystalline-Graphene Oxide Composite. *New J. Chem.* **2018**, *42*, 16682–16693. [[CrossRef](#)]
44. Singh, D.P.; Misra, A.K.; Pandey, K.K.; Pal, B.; Kumar, N.; Singh, D.; Kondratenko, K.; Duponchel, B.; Genevray, P.; Douali, R. Spectroscopic, dielectric and nonlinear current–voltage characterization of a hydrogen-bonded liquid crystalline compound influenced via graphitic nanoflakes: An equilibrium between the experimental and theoretical studies. *J. Mol. Liq.* **2020**, *302*, 112537. [[CrossRef](#)]
45. Lee, J.H.; Lee, J.J.; Lim, Y.J.; Kundu, S.; Kang, S.W.; Lee, S.H. Enhanced contrast ratio and viewing angle of polymer-stabilized liquid crystal via refractive index matching between liquid crystal and polymer network. *Opt. Express* **2013**, *21*, 26914–26920. [[CrossRef](#)]
46. Kumar, P.; Sharma, V.; Jaggi, C.; Malik, P.; Raina, K.K. Orientational control of liquid crystal molecules via carbon nanotubes and dichroic dye in polymer dispersed liquid crystal. *Liq. Cryst.* **2017**, *44*, 843–853. [[CrossRef](#)]
47. Shukla, R.K.; Chaudhary, A.; Bubnov, A.; Hamplova, V.; Raina, K.K. Electrically switchable birefringent self-assembled nanocomposites: Ferroelectric liquid crystal doped with the multiwall carbon nanotubes. *Liq. Cryst.* **2020**, *47*, 1379–1389. [[CrossRef](#)]
48. Uemura, S. Ionic contribution to the complex dielectric constant of a polymer under dc bias. *J. Polym. Sci. Polym. Phys. Ed.* **1972**, *10*, 2155–2166. [[CrossRef](#)]
49. Uemura, S. Low-frequency dielectric behavior of poly(vinylidene fluoride). *J. Polym. Sci. Polym. Phys. Ed.* **1974**, *12*, 1177–1188. [[CrossRef](#)]
50. Yadav, S.P.; Manohar, R.; Singh, S. Effect of TiO₂ nanoparticles dispersion on ionic behaviour in nematic liquid crystal. *Liq. Cryst.* **2015**, *42*, 1095–1101. [[CrossRef](#)]
51. Shin, H.K.; Seo, J.H.; Yoon, T.H.; Kim, J.C.; Woo, H.S.; Shin, S.T. Effects of Pentacene on the Properties of Negative Anisotropy Nematic Liquid Crystal in Vertical Alignment Cell. *Jpn. J. Appl. Phys.* **2009**, *48*, 111502. [[CrossRef](#)]
52. Wrobel, S.; Gestblom, B.; Jadzyn, J.; Kedziora, P.; Hellemans, L.; Wurfinger, A.; Urban, S. Dielectric Relaxation Spectroscopy. In *Relaxation Phenomena*; Springer: Berlin/Heidelberg, Germany, 2003; pp. 13–88. [[CrossRef](#)]
53. Liao, S.W.; Hsieh, C.T.; Kuo, C.C.; Huang, C.Y. Voltage-assisted ion reduction in liquid crystal-silica nanoparticle dispersions. *Appl. Phys. Lett.* **2012**, *101*, 161906. [[CrossRef](#)]
54. Perkowski, P. Dielectric spectroscopy of liquid crystals. Theoretical model of ITO electrodes influence on dielectric measurements. *Opto-Electron. Rev.* **2009**, *17*, 180–186. [[CrossRef](#)]

55. Perkowski, P. Dielectric spectroscopy of liquid crystals. Electrodes resistivity and connecting wires inductance influence on dielectric measurements. *Opto-Electron. Rev.* **2012**, *20*, 79–86. [[CrossRef](#)]
56. Schadt, M. Liquid crystal materials and liquid crystal displays. *Annu. Rev. Mater. Sci.* **1997**, *27*, 305–379. [[CrossRef](#)]
57. Chen, Z.; Jiang, L.; Ma, H. Calculation on frequency and temperature properties of birefringence of nematic liquid crystal 5CB in terahertz band. *Chem. Phys. Lett.* **2016**, *645*, 205–209. [[CrossRef](#)]
58. Prasad, A.; Das, M.K. Optical birefringence studies of a binary mixture with the nematic–smectic Ad-re-entrant nematic phase sequence. *J. Phys. Condens. Matter* **2010**, *22*, 195106. [[CrossRef](#)]
59. Pushpavathi, N.; Sandhya, K.L.; Prasad, S.K. Effect of graphene flakes, titanium dioxide and zinc oxide nanoparticles on the birefringence, I–V characteristics and photoluminescence properties of liquid crystal. *J. Mol. Liq.* **2020**, *302*, 112571. [[CrossRef](#)]
60. Pushpavathi, N.; Sandhya, K.L.; Pratibha, R. Photoluminescence and electrical conductivity measurement of liquid crystal doped with ZnO nanoparticles. *Liq. Cryst.* **2019**, *46*, 666–673. [[CrossRef](#)]
61. Tough, R.J.A.; Bradshaw, M.J. The determination of the order parameters of nematic liquid crystals by mean field extrapolation. *J. Phys.* **1983**, *44*, 447–454. [[CrossRef](#)]
62. Ozbek, H.; Ustunel, S.; Kutlu, E.; Cetinkaya, M.C. A simple method to determine high-accuracy refractive indices of liquid crystals and the temperature behavior of the related optical parameters via high-resolution birefringence data. *J. Mol. Liq.* **2014**, *199*, 275–286. [[CrossRef](#)]
63. Li, J.; Wu, S.T.; Brugioni, S.; Meucci, R.; Faetti, S. Infrared refractive indices of liquid crystals. *J. Appl. Phys.* **2005**, *97*, 073501. [[CrossRef](#)]
64. Selvaraj, P.; Subramani, K.; Srinivasan, B.; Hsu, C.J.; Huang, C.Y. Electro-optical effects of organic N-benzyl-2-methyl-4-nitroaniline dispersion in nematic liquid crystals. *Sci. Rep.* **2020**, *10*, 14273. [[CrossRef](#)]
65. Kalakonda, P.; Basu, R.; Nemitz, I.R.; Rosenblatt, C.; Iannacchione, G.S. Studies of nanocomposites of carbon nanotubes and a negative dielectric anisotropy liquid crystal. *J. Chem. Phys.* **2014**, *140*, 104908. [[CrossRef](#)] [[PubMed](#)]
66. Basu, R.; Kinnamon, D.; Garvey, A. Nano-electromechanical rotation of graphene and giant enhancement in dielectric anisotropy in a liquid crystal. *Appl. Phys. Lett.* **2015**, *106*, 201909. [[CrossRef](#)]
67. Duran, H.; Gazdecki, B.; Yamashita, A.; Kyu, T. Effect of carbon nanotubes on phase transitions of nematic liquid crystals. *Liq. Cryst.* **2005**, *32*, 815–821. [[CrossRef](#)]
68. Reznikov, Y.; Buchnev, O.; Tereshchenko, O.; Reshetnyak, V.; Glushchenko, A.; West, J. Ferroelectric nematic suspension. *Appl. Phys. Lett.* **2003**, *82*, 1917–1919. [[CrossRef](#)]
69. Mrukiewicz, M.; Kowiorski, K.; Perkowski, P.; Mazur, R.; Djas, M. Threshold voltage decrease in a thermotropic nematic liquid crystal doped with graphene oxide flakes. *Beilstein J. Nanotechnol.* **2019**, *10*, 71–78. [[CrossRef](#)] [[PubMed](#)]